

GA-A25659

**QUANTITATIVE RADIOGRAPHY: FILM MODEL
CALIBRATION AND DOPANT/IMPURITY
MEASUREMENT IN CIF ABLATORS**

by

**H. HUANG, R.B. STEPHENS, A. NIKROO, S.A. EDDINGER, K.C. CHEN,
H.W. XU, K.A. MORENO, K.P. YOUNGBLOOD, and M. SKELTON**

JANUARY 2007



DISCLAIMER

This report was prepared as an account of work sponsored by an agency of the United States Government. Neither the United States Government nor any agency thereof, nor any of their employees, makes any warranty, express or implied, or assumes any legal liability or responsibility for the accuracy, completeness, or usefulness of any information, apparatus, product, or process disclosed, or represents that its use would not infringe privately owned rights. Reference herein to any specific commercial product, process, or service by trade name, trademark, manufacturer, or otherwise, does not necessarily constitute or imply its endorsement, recommendation, or favoring by the United States Government or any agency thereof. The views and opinions of authors expressed herein do not necessarily state or reflect those of the United States Government or any agency thereof.

GA-A25659

QUANTITATIVE RADIOGRAPHY: FILM MODEL CALIBRATION AND DOPANT/IMPURITY MEASUREMENT IN CIF ABLATORS

by

H. HUANG, R.B. STEPHENS, A. NIKROO, S.A. EDDINGER, K.C. CHEN,
H.W. XU, K.A. MORENO, K.P. YOUNGBLOOD, and M. SKELTON*

This is a preprint of a paper presented at the 17th Target
Fabrication Specialist Meeting, San Diego, California on
October 1-5, 2006 and to be published in *Fusion Science and
Technology*.

Work supported by
the U.S. Department of Energy
under DE-AC52-06NA27279

GENERAL ATOMICS PROJECT 30272
JANUARY 2007



**QUANTITATIVE RADIOGRAPHY: FILM MODEL CALIBRATION AND DOPANT/IMPURITY
MEASUREMENT IN ICF ABLATORS**

H. Huang,¹ R.B. Stephens,¹ A. Nikroo,¹ S.A. Eddinger,¹ K.C. Chen,¹ H.W. Xu,¹ K.A. Moreno,¹
K.P. Youngblood,¹ and M. Skelton²

¹General Atomics, P.O. Box 85608, San Diego, California 92186-5608

²Massachusetts Institute of Technology, 77 Massachusetts Avenue, Cambridge Massachusetts 02139
huang@fusion.gat.com

In ablator shell fabrication, trace elements and impurities are introduced in the deposition and the pyrolysis process, which must be controlled below a critical level. However, it is the opacity, not the individual elements, which matters in an Inertial Confinement Fusion (ICF) implosion. Radiography measures the opacity, allowing the accurate determination of the total impurity effect in a lump sum. Furthermore, by using the sputter target trace element information, we can determine the radial profile of oxygen to ± 0.4 at. %. Oxygen is very difficult to measure by any other method, but is critically important for beryllium process development such as mandrel removal. To ensure measurement accuracy, we use a local standard to remove fluctuation in film developing and a step wedge to calibrate the film model.

I. INTRODUCTION

Current National Ignition Facility (NIF) target designs are built up of variously doped layers (Fig. 1) which require the radius, the wall thickness and the wall thickness variation of each sublayer to be determined to submicron accuracy. Beryllium is optically opaque which necessitates the use of an x-ray method. Over the last two years, we have developed the imaging equipment and analysis techniques needed to make film-based contact x-radiography quantitative for both dimension and dopant measurements. Accuracy better than required for NIF capsule characterization has been demonstrated.¹ This

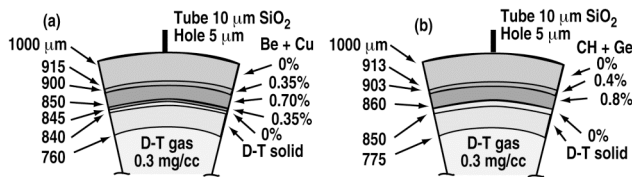


Figure 1. Two alternative NIF target designs utilizing graded ablators: (a) Cu doped Be (b) Ge doped CH. “%” shows atomic fraction of (a) Cu or (b) Ge.

work has also led to a change in the ablator composition requirement, replacing the Z^2 -weighed sum specification with x-ray absorption. This paper updates recent progress in dopant and impurity measurement.

II. EXPERIMENTAL APPARATUS

Our experimental apparatus consists of an x-ray chamber for contact radiography and a digitizer to analyze the film image. A conventional tungsten-anode x-ray tube with 500 μm spot size is used to expose 2 mm sized shells resting on the film plate. The source is placed one meter away in order to reduce the penumbra blurring to $\sim 0.5 \mu\text{m}$. The whole assembly is located in a vacuum chamber to allow low energy photons to propagate without attenuation (Fig. 2). An emulsion-on-glass film plate (Type K1A film from Microchrome Technology, Inc.) is chosen as an x-ray photon detector for its flatness to accommodate the limited depth of field of the digitizer, for its sub-micron grain size to achieve high resolution imaging, and for its enormous dynamic range to capture gray-scale information in a single exposure. (Optical density values from zero to nine have been measured

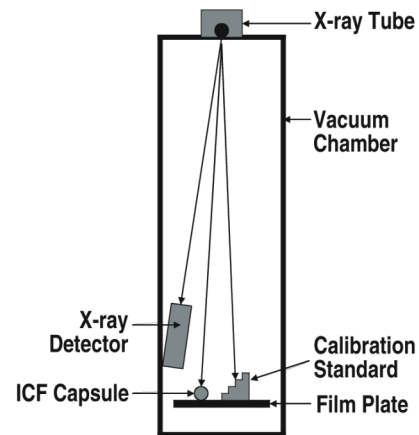


Figure 2. Schematic of the contact radiography system.

which represents the range from full transmission to one in a billion level of photon transmission.) The film image is then digitized by a $2K \times 2K$ Charge Coupled Device (CCD) sensor mounted on a high numerical aperture microscope. The selection criteria for proper digitization equipment and the method to remove pincushion distortion in digitized image were described in an earlier publication.¹

III. FILM MODEL

The x-ray photon detection in the contact radiography system is highly nonlinear, and requires an elaborate film model to convert gray-scale data into dopant or impurity information. For photons with energy E , the film exposure $I(E)$ is proportional to the film spectral sensitivity $F(E)$ and the x-ray transmission along path x , as shown in Eq. (1),

$$I(E) = F(E) \cdot \exp[-\int \mu(E, \rho, Z) dx] \quad , \quad (1)$$

where μ is the material absorption strength, which is a function of photon energy E , material density ρ and elemental composition Z . For a graded shell, μ is a function of the radius. The total exposure is determined by integration over all photon energies, as shown in Eq. (2)

$$I = \int S(E) \cdot I(E) dE \quad , \quad (2)$$

where $S(E)$ is the x-ray spectrum. Based on the total exposure I , the optical density D can be calculated if the film property Φ is known.

$$D = \Phi(I) \quad . \quad (3)$$

By comparing D in Eq. (3) to the measured value, we can determine μ as a function of radius in an iterative process, which gives the dopant concentration profile. Equation (3) is an approximation. Several second order effects, such as reciprocity failure and saturation cannot be properly accounted for in this approach since the spectral sensitivity has been integrated before these corrections could be applied. The presence of soft x-ray photons further complicates the situation because the attenuation in the emulsion is not negligible. The experimentally-derived film spectral and temporal responses should, to some extent, be treated as semi-empirical.

It is evident from this conceptual discussion that the accuracy of the dopant model depends on our knowledge of the x-ray spectrum, its attenuation through the sample and the film response. In this study, we directly mapped the spectra of the W-anode x-ray tube with a Si-detector with the x-ray tube voltages between 4 and 30 kV at 1 kV

interval, a subset of which is shown in Fig. 3. The tungsten M-lines (~ 1.8 keV) and L-lines ($\sim 9-12$ keV) are shown prominently above the bremsstrahlung background. We validated that the x-ray flux can be maintained to a stability level better than $\pm 1\%$ over the course of many months. The plate-to-plate variations in film plate optical density are almost entirely the result of film development process. We will discuss how to calibrate out the variations at the end of this section

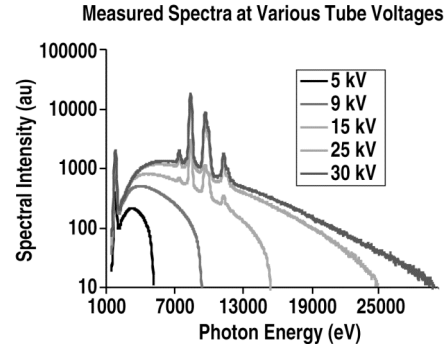


Figure 3. Measured x-ray spectra from a W-anode tube operation between 4 and 30 kV. The spectra displayed here have been corrected for the detector window absorption and the detector quantum efficiency curve. For lithium drifted Si-detectors, the detection efficiency is progressively reduced when the photon energy increases beyond 10 keV.

X-ray attenuation curve of every element in the periodic table is readily available from the online x-ray databases. In this study, we used the one maintained by the Center for X-ray Optics at Lawrence Berkeley National Laboratory (LBNL) which covers a photon energy range from 30 eV to 30 keV.² The x-ray databases are typically based on the best theoretic fit over the experimental data, and are known to be very accurate ($\ll 1\%$) for high Z materials and less accurate (a few percent) for low Z materials. For this reason, we performed additional calibration for beryllium and beryllium oxide after the film model was developed based on the film response to a polypropylene step wedge.

The film properties are by far the most difficult to obtain. Henke, *et al.*³⁻⁵ conducted some pioneering research in film property characterization two decades ago. The semi-theoretically approach would have been of great value; however, the basic information about our film emulsion is not available from either Kodak or its current manufacturer (Microchrome Technology). The lack of information forced us to reverse engineer the film response empirically based on the measurement of optical density after x-ray goes through flat standards such as polypropylene and aluminum step wedges. The film response is shown in Fig. 4.

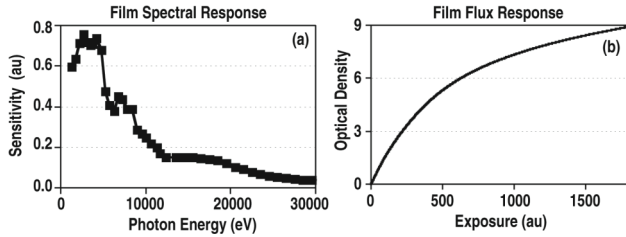


Figure 4. The film response is determined empirically from exposure through step wedge standards.

The accuracy of the film model has been validated against physical standards on all elements relevant to the NIF capsule design. As would be shown later, the sputtered Be shells cannot be used as a Be calibration standard because the absorption level is already greatly elevated due to the presence of contaminants such as oxygen. For the calibration of beryllium and oxygen, we purchased highest purity beryllium and beryllium oxide flats from GoodFellow Incorporated. The trace element certificate allows the absorption effect from the small amount of trace elements to be accurately accounted for. The flat thicknesses measured from the film optical densities and calculated by the film model agree to the physical thicknesses calculated from weight and dimension measurement (Table I). Because x-ray absorption follows the well known exponential decay formulary, the measurements on pure beryllium and pure beryllium oxide standards validates the film model on beryllium with any atomic percent of oxygen. Following the same approach, we used a 1–6 μm thick copper step wedge to calibrate the film model. The copper thicknesses were chosen to cover the entire copper dopant range in a NIF capsule where 0 to 0.75 at. % copper is to be distributed along an $\sim 1000 \mu\text{m}$ x-ray path length. The copper step wedge thicknesses measured from radiography agrees with the copper physical thicknesses as shown in Fig. 5. The use of physical standards allows the film model to be calibrated to $<5\%$ accuracy, which is at least a factor of two better than possible by directly comparing against other micro-analysis methods. These methods, such as X-ray Fluorescence (XRF) and Energy-Dispersive Spectroscopy (EDX),¹ each has an error $\sim 10\%$.

Table I. Pure Be and BeO Flat Standards are Used to Calibrate the Film Model

Sample	Thickness (mm)	Measurement (mm)	Difference (%)
Be	541	527	2.6
Be	1082	1086	-0.4
BeO	507	481	5.1

The flat standard approach can be used in reverse to measure the equivalent exposure. Even with tight control of x-ray flux, which is verified by x-ray detector to vary

less than $\pm 1\%$, the optical density from film plate to film plate tends to vary by as much as $\pm 25\%$, and by $\pm 10\%$ within each film plate. The variations are almost entirely due to the film processing, which is sensitive to factors such as the freshness, the concentration, and the temperature of the chemicals; the strength and duration of agitation; the number and the spacing between the film plates within each batch and their locations within the bath. Furthermore, we cannot rely on the optical density saturation to reduce the time dependence of film processing: We have experimentally determined that the optical density of this film increases linearly with the developing time between 1 and 8 minutes. (5 minutes recommended by the manufacturer.) For a typical film exposed for 40 min under 9 kV, 7 mA tube condition, every second submerged in the developer reduces the film transmission by $\sim 3\%$. A ± 5 s operator error leads to ± 0.07 change in film optical density. The widely varying process conditions can be effectively corrected by physical standards. The use of a polypropylene step wedge can reduce uncertainty in absorption measurement to $\pm 10\%$, and the use of a PAMS ball standard in close proximity of the sample (*i.e.* within the same XRF holder) further reduces the uncertainty to $\pm 2\%$.

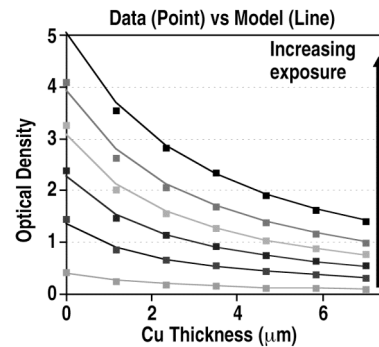


Figure 5. A copper step wedge is used to calibrate the film model. The dots are the physical thicknesses plotted against the measured optical densities. The lines are the thicknesses calculated by the film model based on the measured optical densities. The film model is accurate over a wide range of exposure times, each of which is represented by a curved line.

IV. MEASUREMENT SENSITIVITY

Contact radiography in conjunction with the film model measures the absorption level of a sample to an accuracy of $\pm 5\%$ and repeatability of $\pm 2\%$. This translates into different measurement sensitivities for different elements, as shown in Table II for the three most common ingredients in a sputtered beryllium.

Contact radiography determines the dopant/impurity levels by comparing the measured radial transmission

profile to the simulation profile calculated from a film model. To avoid rigorously computing the infinite combinations of trace elements that can give rise to the measured absorption, we need to develop a simpler method to evaluate the relative sensitivity of each element. For the same atomic concentration, the absorption ratio between two elements, such as O/Be=20 or Ar/Be=430, is a useful concept, but it must be treated with caution to avoid gross error. Strictly speaking, there is no fixed ratio between two element sensitivities, because the ratio depends on (1) the base material type (2) the aerial density (that is, the density times the thickness), (3) the x-ray spectrum and the x-ray film used in the measurement.

Table II. 1- σ measurement repeatability and accuracy for three elements. It is worth noting that argon (Z=19) is a lighter element than copper (Z=29), yet the detection limit is lower. The break down of Z^2 scaling law in radiograph sensitivity will be explained later

	Precision	Accuracy
Oxygen	± 0.1 at. %	± 0.4 at. %
Copper	± 0.008 at. %	± 0.02 at. %
Argon	± 0.005 at. %	± 0.01 at. %

As shown in Figs. 6 and 7, depending on the location of the absorption edge, the behavior of an element in beryllium can be dramatically different. On one extreme are elements such as oxygen and copper which do NOT have any absorption edge within the measurement spectrum range of ~ 1.5 –8 keV. The absorption ratio between oxygen and beryllium is relatively unchanged regardless of the thickness of the sample. The ratio varies from 17 for a 1 μm thick sample to 20 for a 1000 μm thick sample. On the other extreme are elements such as argon and calcium which do have prominent K-edge in the middle of the spectrum. The absorption ratio between argon and beryllium varies from 85 for a 1 μm thick sample to 440 for a 1000 μm thick sample. In a thick sample, the low energy photons were filtered out by bulk beryllium whereas the high-energy photons were filtered out by the argon impurity. The two elements serve as a complementary filter pair to achieve maximum attenuation. As a result, even though argon (Z=18) is lighter than copper (Z=29), the contact radiograph is more sensitive to argon (Table II). The usual Z^2 scaling law for x-ray opacity breaks down. The changing absorption ratio makes the concept less useful for Ar, however, we can define an “effective” absorption ratio relevant to the shells we measure.

We define a ratio based on infinitesimal variations in impurity elements: In a base material such as full density beryllium ($\rho=1.848$ g/cc) with a given thickness such as 1000 μm , what is the ratio between trace elements 1 and 2 (in infinitesimal quantities) to produce the same measur-

able effect in radiography? The result is tabulated in Table III for every element in the periodic table for the NIF relevant X-ray path length of 1000 μm in beryllium. The range of X-ray path length varies from 300 μm to 1054 μm when the X-ray cut through a shell at a depth exceeding 10 μm . Under this condition, the typical variation of the absorption ratio is $\pm 10\%$ (shown as the absorption ratio range for each element in Fig. 7), which represents the calculation error using this simple concept.

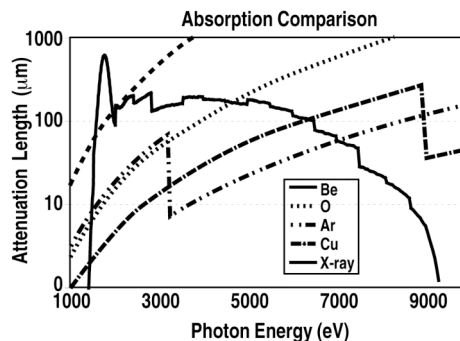


Figure 6. The attenuation length for each element at a density of 1 g/cc is plotted against the “x-ray” curve. The “x-ray” curve is the product of the x-ray spectrum (tungsten tube operated at 9 kV) and the x-ray film spectral sensitivity. The curve is an effective measurement of how the x-ray photons of different energies contribute to the film exposure. A shell can be viewed as a filter, with each of the trace elements further attenuating the curve.

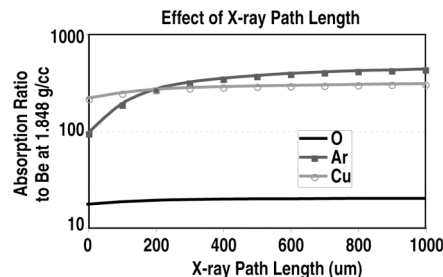


Figure 7. For a given base material, x-ray spectrum and x-ray film, the absorption ratio between two elements can be defined as a function of x-ray path length. The definition here is based on how much the x-ray absorption changes with an infinitesimal variation in the trace level of one element. The elements with steeper slopes are the ones that have absorptions edges in the middle of the measurement spectrum range (Fig. 6).

The absorption ratio concept makes the impurity elements interchangeable in absorption calculation. It enables a user to estimate the effect of trace element without specialized tools. Because an infinite variety of impurity element combinations that can give rise to the same observed absorption profile, such back-of-the-

Table III. The absorption ratios of trace elements in full density beryllium ($\rho=1.848\text{g/cc}$). All values references to beryllium which by definition has an absorption level of one. This absorption ratio table empowers the user to quickly estimate, to a typical 10% accuracy, the absorption contribution due to a trace element when the atomic percent concentration is known. For example, if there is 1 at. % oxygen, the absorption level will increase by 19.7%. The values are calculated for an x-ray path length of 1000 μm which is representative to that in a shell. The calculation assumed Type K1a film plate and a W-anode tube operating at 9 kV

Element	Ratio	Element	Ratio	Element	Ratio	Element	Ratio
H	9.90E-03	Cr	3.31E+02	Ag	1.84E+03	Yb	2.07E+03
He	4.15E-02	Mn	3.13E+02	Cd	1.96E+03	Lu	2.21E+03
Li	2.42E-01	Fe	2.87E+02	In	1.95E+03	Hf	2.30E+03
Be	1.00E+00	Co	2.69E+02	Sn	1.99E+03	Ta	2.41E+03
B	2.57E+00	Ni	2.80E+02	Sb	1.90E+03	W	2.54E+03
C	5.87E+00	Cu	3.03E+02	Te	2.02E+03	Re	2.67E+03
N	1.10E+01	Zn	3.46E+02	I	1.89E+03	Os	2.81E+03
O	1.97E+01	Ga	3.92E+02	Xe	1.87E+03	Ir	2.99E+03
F	3.13E+01	Ge	4.49E+02	Cs	1.79E+03	Pt	3.16E+03
Ne	4.73E+01	As	5.10E+02	Ba	1.80E+03	Au	3.37E+03
Na	6.73E+01	Se	5.75E+02	La	1.79E+03	Hg	3.51E+03
Mg	9.75E+01	Br	6.45E+02	Ce	1.71E+03	Tl	3.65E+03
Al	1.27E+02	Kr	6.98E+02	Pr	1.66E+03	Pb	3.82E+03
Si	1.69E+02	Rb	7.81E+02	Nd	1.66E+03	Bi	3.95E+03
P	2.24E+02	Sr	8.86E+02	Pm	1.63E+03	Po	4.10E+03
S	2.77E+02	Y	9.75E+02	Sm	1.71E+03	At	4.34E+03
Cl	3.45E+02	Zr	1.09E+03	Eu	1.63E+03	Rn	4.55E+03
Ar	4.28E+02	Nb	1.20E+03	Gd	1.76E+03	Fr	4.68E+03
K	4.87E+02	Mo	1.30E+03	Tb	1.64E+03	Ra	4.80E+03
Ca	4.93E+02	Tc	1.39E+03	Dy	1.68E+03	Ac	4.85E+03
Sc	4.73E+02	Ru	1.51E+03	Ho	1.84E+03	Th	5.03E+03
Ti	4.10E+02	Rh	1.67E+03	Er	1.85E+03	Pa	5.28E+03
V	3.76E+02	Pd	1.77E+03	Tm	1.98E+03	U	4.71E+03

envelop calculation offers great insight to complex processing issues, such as how much more oxygen an implosion can tolerate when the argon content is suppressed by a set of sputter conditions. It also allows the NIF trace element specification to be rewritten into a functional equivalent format that simplifies the production measurement.

V. TRACE ELEMENT SPECIFICATIONS

The original trace element specification was written as the sum of $0.01 \cdot \text{at. \%} \cdot Z^2$ not to exceed 0.2 for all trace elements (except for oxygen and argon). Up to 0.8 at. % oxygen and up to 0.1 at. % argon are allowed, which contribute to 0.51 and 0.33 respectively to the $0.01 \cdot \text{at. \%} \cdot Z^2$. Oxygen and argon were separately treated mainly for their abundance. The essence of the specifications is to limit the lumped effect of all impurities to a low enough level so that the copper dopant dominants the

absorption profile. How the trace element concentrations are partitioned is not important.

The Z^2 scaling factor is an approximation, true only if the elements do not have absorption edges. The diversity of trace elements tends to average out these variations (Fig. 8). In other words, the $0.01 \cdot \text{at. \%} \cdot Z^2$ sum is a simplified description of x-ray absorption with perhaps $\pm 30\%$ accuracy.

As shown in Fig. 8, the trace elements levels for four types of commercial berylliums were provided by the manufacturers. The heavier elements were measured by the Inductive Coupled Plasma-Optical Spectroscopy (ICP-OES) and the oxygen was measured by a fusion method developed by LECO Corporation (which melts beryllium in graphite crucible and measures the carbon monoxide and dioxide emission), both of which are destructive techniques that consume grams of materials

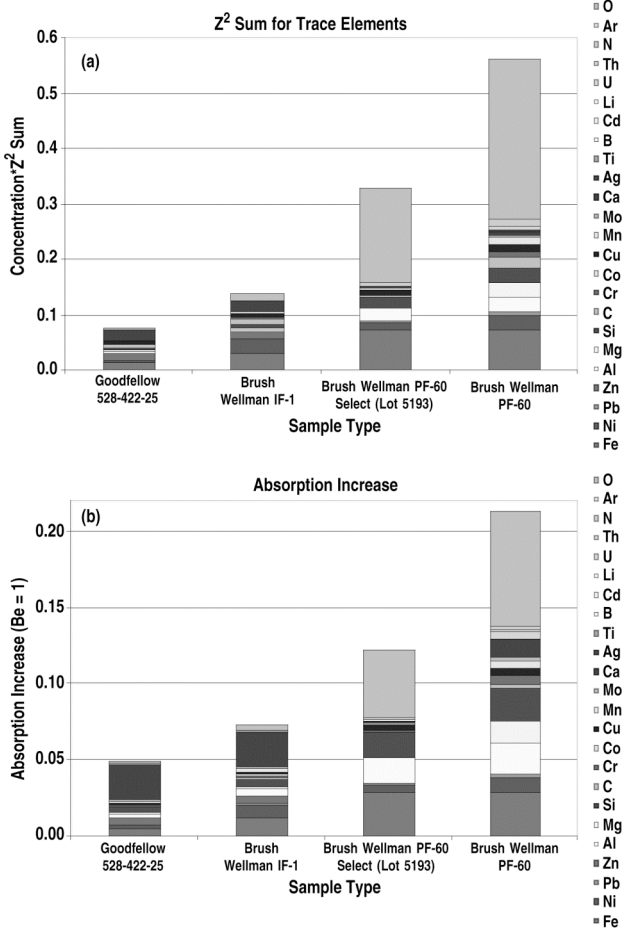


Figure 8. Even though each trace element contributes to the $0.01 \text{ at. \%} \cdot Z^2$ specification (a) in a different proportion to the absorption increase (b), the diversity of trace elements tends to average out the individual differences, and produce good linearity between the two sums. The linear scaling enables the rewrite of the trace element specifications in terms of the overall absorption increase; making it easier to conduct non-destructive measurements. In (a) and (b), the legend is in the same descending order as the elements in the bar graph. In particular, there is a fair amount of oxygen expected in the PF-60 grade (the light gray element on top of the bar) which is used for sputter targets.

(which equal in weight to a few hundreds of shells therefore not practical on production capsules). The values were plotted in $0.01 \text{ at. \%} \cdot Z^2$ format in (a) and in absorption increase format in (b). The good overall linear scaling enabled the rewrite of the trace element specs in terms of the overall absorption increase; making it possible to conduct non-destructive radiography measurement on production capsule. The PF-60 grade beryllium from Brush Wellman, which is shown in Fig. 8 as the third and the fourth columns, is the sputter target material used in Be shell production. It is evident that the trace elements in

the beryllium target, excluding oxygen, barely make the 0.2 trace element specs and contribute to about a $10\% \pm 3\%$ increase in absorption.

The new NIF impurity specifications lump oxygen with other trace elements and are given a total allowance of 30% absorption increase. Argon, which is easily measured by XRF, is still treated separately and given an allowance of 0.1 at. %. A 30% criterion is an exact equivalent of the original specification. Argon is separated for its potential abundance under biased deposition conditions and for its abnormal sensitivity with respect to the x-ray spectrum used in the measurement (Fig. 6). When no bias is used, the actual argon concentration is typically measured around 0.007 at. %, which with an absorption ratio of 430x, contributes to a mere 3% absorption increase. Under such a circumstance, argon does not have to be separated out, and the total impurity specifications can potentially be relaxed a little without sacrificing implosion performance. Such a trade-off is of importance, because the as-deposited shells typically have an absorption level 30%-45% higher than that of pure Be.

There are several advantages to the new impurity specifications:

1. We can now non-destructively measure the sample to be shot, instead of measuring the sputtering target.
2. Radiography measures opacity with the same Z^2 scaling factor with element as during implosion. What is not seen is irrelevant to the implosion performance.
3. Oxygen, which is extremely difficult to measure even with the destructive methods, can now be calculated to ~ 0.4 at. % accuracy. Such information is helpful to process development, and will be discussed in the next section.

VI. OXYGEN PROFILING

The procedure established in Sec. III can be used for oxygen estimation in a shell. For a shell with 40% absorption increase beyond pure beryllium, subtracting the 3% contribution from argon and the $\sim 10\%$ contribution from other trace elements, the remaining 27% absorption increase can be attributed to ~ 1.4 at. % oxygen. Using this approach, we have observed that as-deposited shells fresh from the sputter chamber; the oxygen level is typically ~ 1 at. %. As the shells sit in the air for weeks, the opacity increases by $\sim 10\%$ which corresponds to ~ 0.5 at. % oxygen pick-up. The weight of the beryllium layers also increase by $\sim 1\%$ over the same period. The only element in the periodic table to simultaneously increase the weight by $\sim 1\%$ and the absorption by $\sim 10\%$ is oxygen. The

absence of carbon and nitrogen (proven by EDX and Rutherford Backscattering measurement) ruled out the possibility that a mixture of low Z and high Z element pick-up could produce the correct signature: Any high Z element would increase the weight much less than ~1% if it causes a 10% increase in absorption.

We can take this approach further to determine the oxygen profile in the shell. Figure 9(a) is a typical before and after pyrolysis radial profile of a beryllium shell. Two changes occurred during pyrolysis: (1) The CH layer was prominent in the before case and is missing in the after case. (2) The Be layer allowed a lesser amount of x-rays to pass through, resulting in a less exposed film image or a more transparent radial profile. Film model was used to fit the observed profiles in Fig. 9(a), and gave the x-ray absorption profiles shown in Fig. 9(b). The Be layer is 94.7% dense. If only Be is present, the shell should have an absorption level of 0.947 when compared to full density pure Be, which is shown as a horizontal line at the bottom of Fig. 9(b). The absorption level before pyrolysis was measured a dozen times on several samples from the same batch, and plotted as horizontal lines around 1.36 in Fig. 9(b). The 44% absorption increase suggests the oxygen level is ~1.5 at. % before pyrolysis. The $\pm 2\%$ spread between the lines indicates the $1-\sigma$ repeatability of absorption measurement. The vertical lines on the left is the interface between CH and Be. CH is more than twice as absorbing as Be and is shown as a greatly elevated line at the far left in Fig. 9(b). Also plotted are the post-pyrolysis shells, in which 3 features are prominent: (1) The CH removal is complete enough that no residue is visible on the radiography to affect the radial transmission profile. (2) The absorption profile has a steep gradient. (3) The absorption level in the inner 7 μm beryllium layer remains unchanged after pyrolysis. Figure 9(c) shows the oxygen profile obtained from Fig. 9(b) for the post-pyroed shells together with the measurement obtained from EDX on a cross-section sample.

As demonstrated in Sec. II, the oxygen measurement was calibrated for the entire range 0 to 50 at. % by the use of Be and BeO flats. Additional validation pertinent to the shell measurement is possible by weighing, and by EDX. In Fig. 9(b), the before and after absorption profile change integrates to an 2.73 at. % oxygen increase, whereas the net density gain from weight measurement suggests a 2.52 at. % oxygen increase. Such comparisons were made on many shells of different types, the correlation is typically better than 10% of the reported value.

To validate the steep oxygen profile shown in Fig. 9(c), we conducted EDX measurement on cross-section samples. The most reliable matrix we developed is the O/Be peak ratio, because the height of either the

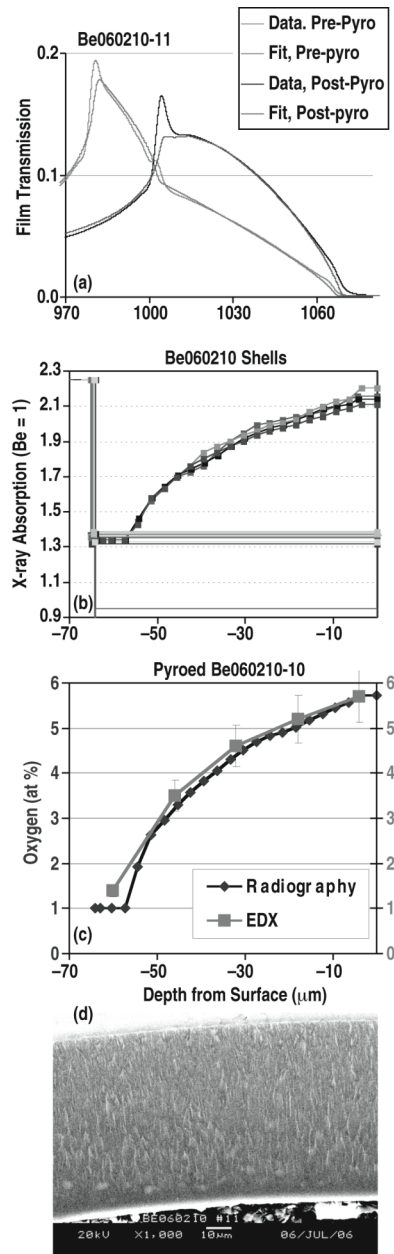


Figure 9. Oxygen profile (c) is determined from the absorption profile (b) which in turn is determined from the shell radial profile (a) measured from the film plate. The average oxygen increase before and after pyrolysis can be validated by weight measurement. The non-uniform distribution of oxygen can be validated by EDX measurement on cross-section sample. In both cases, the agreement is within 10% of the reported values. Polished cross-section is featureless in secondary electron image (not shown) but has pronounced contrast in backscattered electron image (d) in a texture consistent with grain-boundary oxidation. The first 7 μm , devoid of visible grain structure, is also the layer that does not have additional oxygen pick-up (c).

oxygen peak or the beryllium peak are greatly influenced by the topology of the fractured surface. For a given Scanning Electron Microscopy (SEM) condition, such as the 20 keV electron probe energy we used, each value of the O/Be peak ratio corresponds uniquely to an oxygen atomic percent, even though the correlation is nonlinear. We have established a simple physics model to convert the O/Be peak ratio into oxygen atomic percent. The model assumes that (1) e-beam generates x-ray fluorescence uniformly in the first 4 μm of the sample (which agrees reasonably well with the CASINO simulation) and (2) the integrated fluorescence line intensity from all depths (after attenuation) determines the measured peak intensity. There is only one free scaling factor in this model, which has to do with the detailed design of the x-ray detector, the sampling geometry and the fluorescence yield. If we pick the scaling factor consistent with the weight gain measurement, the EDX oxygen profile quantitatively agrees to the radiography measurement to within an error of 10%, as shown in Fig. 9(c). It is remarkable that the same model, with the same scaling factor, fit all the shells we have measured so far with the radiography method, even though these shells have vastly different oxygen profiles due to different deposition and annealing conditions (Fig. 10). We also performed EDX measurements on the polished cross-section of the same sample. The same oxygen gradient was confirmed, although the entire profile is raised by a fraction of a percent, perhaps due to surface oxidation in sample polishing. Backscattered electron imaging confirms the oxygen distribution in Be is heterogeneous in a pattern resembling the grain structure [Fig. 9(d)]. Relatively easy transportation of oxygen atoms to grain boundary sites is accomplished through a network of interconnected nano-cracks at the (otherwise impermeable) grain boundaries. The oxygen diffusion through the existing oxide layer at interior (open) grain boundary sites is the rate-limiting step, which leads to a relatively flat plateau toward the outside surface [Fig. 9(c)]. In other word, the oxide forms a self-passivating layer: The oxygen source is outside the shell. Longer exposure (and perhaps at higher oxygen concentration) on the Be layer near the external surface does not significantly increase the oxygen content.⁶

The nondestructive oxygen profiling capability provides valuable process development feedback. Figure 11(a) shows the effect of pyrolysis temperature on oxygen pick-up. Even at room temperature, the shells pick up weight which is interpreted as picking up oxygen. The oxygen level saturates at ~ 1.5 at. %. 100°C processing, which is not effective in removing the CH mandrel, increases the oxygen further. At temperatures above 400°C , for duration sufficient to remove the CH mandrel, the actual processing temperature or duration does not lead to much difference in the oxygen increase. Rather, the porosity of the beryllium plays a much more dominant

role in oxygen (and thereby weight) increase. As shown in Fig. 11(b), the density gain correlates well to the pre-pyro density, even though these hundreds of shells were pyroed under a variety of different anneal conditions (that were sufficient for full mandrel removal).

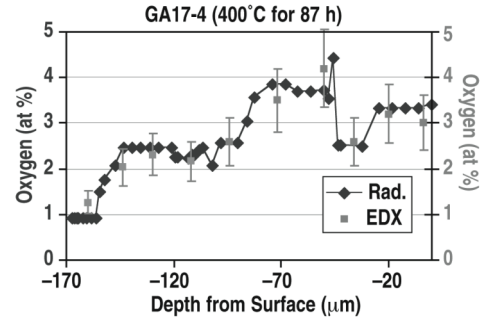


Figure 10. Oxygen profile of NIF graded shell design after being pyrolyzed at 400°C for 87 h in air. EDX measurement again agrees with the radiography measurement (as does the weight measurement, which is not shown).

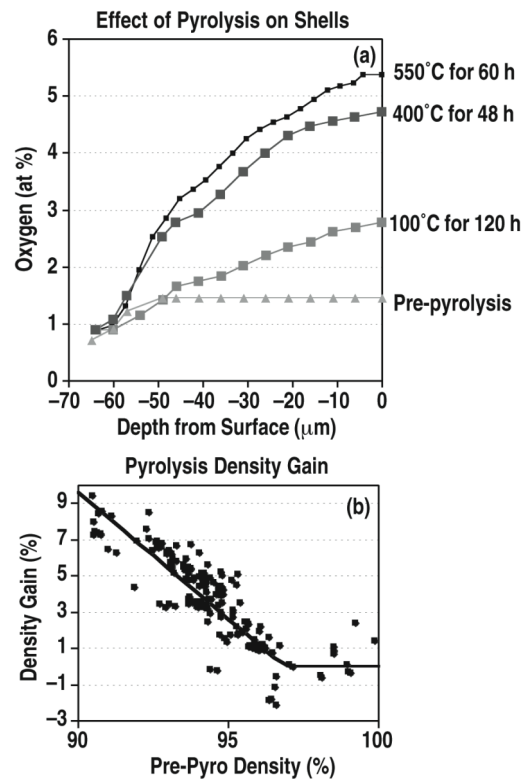


Figure 11. Pyrolysis temperature affects the oxygen pick-up (a). However, effective CH removal requires temperatures above 400°C . Within that temperature constraint, the porosity of the shell plays a much more dominant role (b).

The oxygen profile measured by radiography does offer a plausible solution to this pesky oxygen problem. In

most (but not all) types of beryllium shells, oxygen can not penetrate the innermost 7–12 μm of the beryllium, resulting in an unperturbed layer after pyrolysis, as shown in Fig. 9(c) and Fig. 10. It is therefore possible to deposit a \sim 5–10 μm beryllium layer, remove the CH mandrel by pyrolysis, followed by full thickness coating with the initial beryllium layer serving as the mandrel. The later beryllium layer has no need for thermal processing, whereas the earlier layer does not have oxygen pick-up even with thermal processing. As a result, the entire shell should meet the NIF impurity specifications. Limited experiments have been performed, with good results.

VII. SUMMARY

Film-based contact radiography has matured into a production-worthy tool for NIF capsule metrology. We have established a versatile film model to convert gray-scale measurement on a film plate into dopant and impurity profiles to guide process development work in beryllium capsule fabrication. We have also established an absorption ratio concept that enables the trace element specifications to be validated non-destructively on production samples.

ACKNOWLEDGMENT

This work is supported by the US Department of Energy under DE-AC52-06NA27279. The authors thank D. Wall of General Atomics for the EDX measurements, S. Haan of Lawrence Livermore National Laboratory for the discussion that led to the rewrite of the trace element specifications, and J. Knauer of University of Rochester

for introducing us to x-ray spectrum measurement using Si(Li) detector.

REFERENCES

1. H. HUANG, R. B. STEPHENS, S. A. EDDINGER, A. NIKROO, K. C. CHEN, H. W. XU, J. GUNTHER, “Non-destructive Quantitative Dopant Profiling Technique by Contact Radiography,” *Fusion Sci. Technol.* **49**, 650 (2006).
2. http://www.cxro.lbl.gov/optical_constants/atten2.html
3. B. I. HENKE, S. L. KWOK, J. Y. UEJIO, H. T. YAMADA, G. C. YOUNG, “Low-Energy X-ray Response of Photographic Films. I. Mathematical Models,” *J. Opt. Soc. Am. B* **1**, 818 (1984).
4. B. I. HENKE, F. G. FUJIWARA, M. A. TESTER, “Low-Energy X-ray Response of Photographic Films. II. Experimental Characterization,” *J. Opt. Soc. Am. B* **1**, 828 (1984).
5. B. I. HENKE, J. Y. UEJIO, G. F. STONE, C. H. DITTMORE, F. G. FUJIWARA, “High-Energy X-ray Response of Photographic Films. Models and Measurement,” *J. Opt. Soc. Am. B* **3** (11), 1540 (1986).
6. C. TOMASTIK, W. WERNER, H. STORI, “Oxidation of Beryllium—a Scanning Auger Investigation,” *Nucl. Fusion* **45**, 1061 (2005).